UCRL-CR--104934

DE91 000814

# PHOTOCONDUCTIVITY OF ACTIVATED CARBON FIBERS

K. Kuriyama
M. S. Dresselhaus

MIT
Cambridge, Massachusetts



August 1990

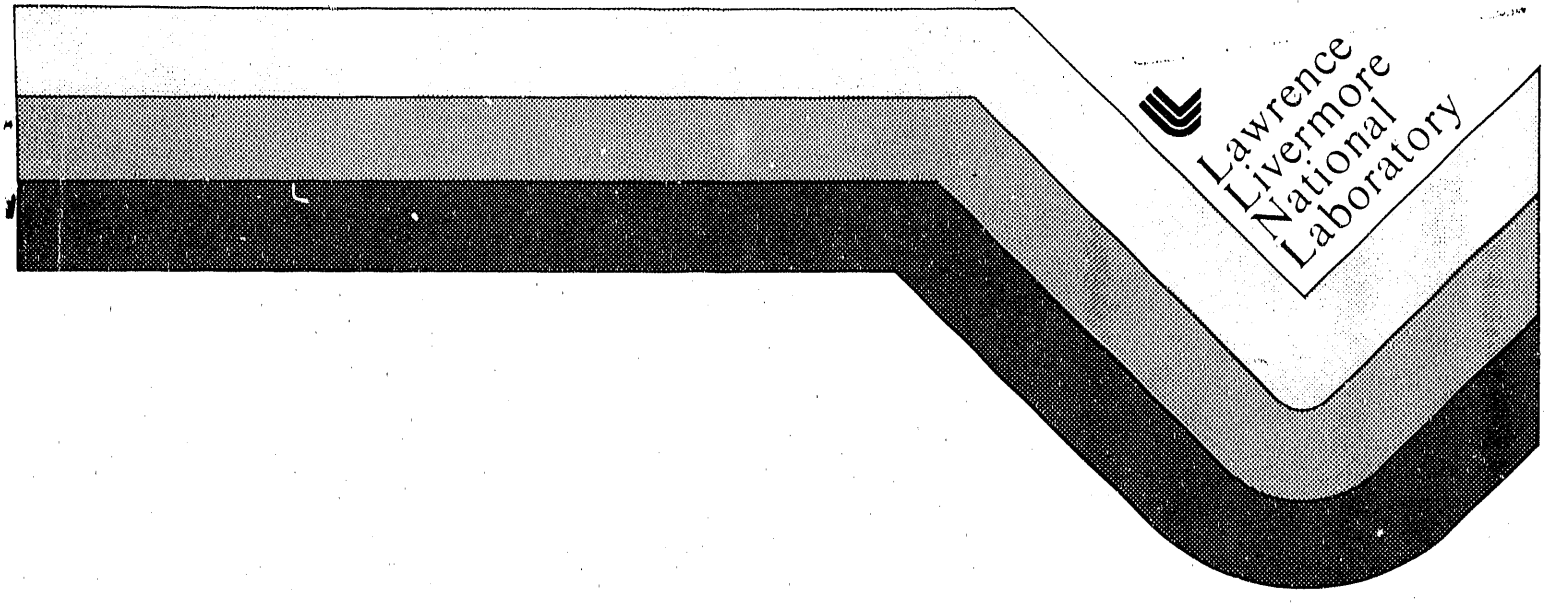

## DISCLAIMER

# Photoconductivity of Activated Carbon Fibers

K.Kuriyama[+] and M.S.Dresselhaus
Department of Electrical Engineering and Physics
Massachusetts Institute of Technology, Cambridge, Massachusetts 02139

The photoconductivity is measured on a high-surface-area disordered carbon material, namely activated carbon fibers, to investigate their electronic properties. Measurements of decay time, recombination kinetics and temperature dependence of the photoconductivity generally reflect the electronic properties of a material. The material studied in this paper is a highly disordered carbon derived from a phenolic precursor, having a huge specific surface area of 1000-2000$m^2/g$. Our preliminary thermopower measurements suggest that this carbon material is a p-type semiconductor with an amorphous-like microstructure. The intrinsic electrical conductivity, on the order of 20S/cm at room temperature, increases with increasing temperature in the range 30-290K. In contrast with the intrinsic conductivity, the photoconductivity in vacuum decreases with increasing temperature. The recombination kinetics changes from a monomolecular process at room temperature to a bimolecular process at low temperatures. The observed decay time of the photoconductivity is $\simeq$0.3sec. The magnitude of the photoconductive signal was reduced by a factor of ten when the sample was exposed to air. The intrinsic carrier density and the activation energy for conduction are estimated to be $\simeq 10^{21}/cm^3$ and $\simeq$20meV, respectively. The majority of the induced photocarriers and of the intrinsic carriers are trapped, resulting in the long decay time of the photoconductivity and the positive temperature dependence of the conductivity.

## I. Introduction

Study of the electronic properties of disordered systems is currently an area of active interest. In the case of carbon materials, interesting phenomena have been observed in some disordered carbons, such as Saran carbon

rods(in terms of their conductivity[1]), active carbon rods(in terms of their resistivity[2,3]), evaporated carbon films(in terms of their resistivity[4,5], photoconductivity [6], optical absorption edge [7], adsorption [8,9] and ESR [10]), anthracite carbon powders ( in terms of their electrical properties [11] ), glassy carbons [12-14] and others [15-20]. A series of systematic investigations on the electronic properties of various types of carbon materials have been carried out by Mrozowski[21-27].

Activated carbon fibers(ACFs) are expected to show electronic behavior characteristic of disordered systems, since ACFs are a highly disordered carbon material. As shown in a B.E.T measurement of other activated carbon materials[1], every second atom can be a surface atom that has a dangling bond. Thus activated carbon is regarded as a good material for research on strongly disordered systems. However, few electronic properties of ACFs have been reported, though their adsorption properties have been extensively investigated [28-41]. The adsorption rate of the ACFs is 100-1000 times faster than granular-type activated carbons and the adsorption capacity is ten times greater than that for the granular-type[33]. An electric double layer capacitor [34] is an example of an application taking advantage of the huge specific surface area of ACFs.

The fibers of the present study are derived from phenol, one of four precursors used to prepare ACFs: PAN[28,29], cellulose[30], pitch[31] or phenol [32,33]. To prepare the ACFs, these precursors are activated at temperatures 1100-1400K in $O_2$, $H_2O$, $CO_2$ or other oxidizing atmospheres[34-38]. In contrast with usual heat treatments, the consequence of this heat treatment is to form more disorder in the material. The specific surface area is controlled by changing the temperature and the time for the activation process. The maximum specific surface area is about $2800m^2/g$ in commercial activated carbon fibers [33]. Among these ACFs, the phenol-derived fibers studied in this paper have a relatively high strength, a large specific surface area and require a simple process for activation[33]. They have a diameter of around $10\mu$, a conductivity of the order 20S/cm at room temperature and a specific surface area in the range $1000-2000m^2/g$.

In this work, photoconductivity was used as one of the main techniques to characterize the ACFs, since photoconductive measurements have several advantages over other characterization techniques. If the density of photocarriers is known, the density of intrinsic carriers can be estimated based on the recombination kinetics. The existence of trap states is inferred by the observation of decay time. General concepts are described in details in several monographs on photoconductivity and related phenomena[42-44]. Thus photoconductive data give information necessary to describe the electronic properties of the material.

For ACFs, photoconductive measurements are particularly useful as a characterization technique for the following reasons. Measurement of the Hall effect, which is usually a useful technique to determine the type of carriers and their density, is not feasible because of the very small diameter of the ACFs. Even if the measurement were possible, good data would not be expected because the mobility in such a disordered material should be very small. Because of the high degree of disorder of these fibers, other measurement techniques like Raman scat ering, magnetoresistance and thermoelectric power give only qualitative comparisons among the fibers.

In this paper, we firstly report the results of the conductivity and the photoconductivity measurements of the activated carbon fibers. Then the conduction mechanism is discussed based on the temperature dependence. The long decay time of the photoconductivity contributes to the discussion as evidence of a high density of trap states. The change in the recombination kinetics supports an argument that the conductivity increase is not a thermal effect but a photoeffect. In the final section, we quantitatively fit the conductivity data to functional forms appropriate to consider the conduction mechanisms.

## II. Samples and Experimental Details

A single phenol-derived activated carbon fiber(supplied by Kuraray Chemical Co.), with properties listed in Table 1[33], is mounted on a mica substrate

for conductivity measurements. The specific surface area of these fibers is derived from the last two digits of the fiber name when multiplied by 100 in units of $m^2/g$(see Table 1). The mica substrate was set on a copper heat sink that was suspended onto a cryo-stage of an Air Products Cryogenics closed cycle He refrigerator (see Fig.1). To measure the sample temperature, a thermometer was mounted on the opposite side of the copper heat sink. Electrical contact to the fibers was made with silver paint and four 0.5mm diameter copper wires were thus attached for electrical contacts. A dc four-terminal method was used for the conductivity measurements with a constant 1μA or 10μA current source. The effect of the temperature rise due to Joule heating was negligible because the measurements showed the same resistivity at 30K over the whole current range 0.1-10μA that was measured. The current direction was reversed during the measurements to check for possible thermoelectric effects in the contacts.

The inside of the system was pumped down to $10^{-3}$ Torr at room temperature to reduce the effects of gas adsorption, since in a preliminary measurement a remarkable decrease in photoconductivity was observed for ACFs exposed to air. In air, the room temperature photoconductivity diminished by a factor of at least 10, compared to vacuum, although the intrinsic conductivity showed almost no change between exposure to air or vacuum. We interpret this result to indicate that the adsorption of gas molecules interacts with localized recombination centers and accelerates the recombination process, resulting in a decrease in the photocarrier lifetime. This adsorption seems to be a physisorption process because the change in the photoconductivity was observed to be reversible. Effects of oxygen and water vapor have been investigated in terms of gas adsorption on carbon materials [2,3,8,9], where the intrinsic resistivity generally increased as a result of adsorption. In our experiments, water vapor is the most probable gas which changes the photoconductivity of the ACFs reversibly at room temperature because reversible physisorption usually occurs at temperatures below the boiling point of the adsorbates. Besides that, the effect of nitrogen is known to be negligible and oxygen is known to cause an irreversible chemisorption at room temperature[8]. On the

other hand, a change in the intrinsic resistivity was observed when a fiber was baked in air at around 300°C. The resistivity decreased 10-15% as a result of the baking and the room temperature resistivity slowly returned to the initial value after exposure to air for one day. Thus the chemisorption of oxygen, which is not removed by pumping down, is indicated to take place in the ACFs. Our experimental results therefore show some effects relevant to oxygen adsorption or surface oxidization.

Scanning electron microscopy(SEM) was used to determine the fiber diameters and to observe the macrostructure of the fibers. The SEM results of Fig.2. for FR12, which has a specific surface are of $1200m^2/g$, show macroscopic pores in the ACFs with openings of about 500Å. Besides the macroscopic pores, the ACFs have microscopic pores with mean radii listed in Table 1(obtained by the water vapor adsorption method [33] ). As seen in Fig.2, the fibers have a rather regular round cross section and a smooth surface.

The diffraction pattern for ACFs(Fig.3) is broad, indicating an amorphous-like microstructure. An estimate for $L_c$ of about 10Å(about three interlayer spacings, about the same length as for Saran carbon[1]), was obtained from the linewidth of the (002) X-ray diffraction line for phenol-derived ACFs with a specific surface are of $1200m^2/g$.

We determined the dominant conduction type as p-type at room temperature by a rough measurement of the thermoelectric power, which was found to be small. The high temperature terminal in this measurement showed a negative potential(i.e., carrier type is positive) and the thermoelectric power was found to be about 1.7μV/K at room temperature. Highly disordered carbon materials are known to be usually p-type[45,46].

In the photoconductive measurements, an Ar ion laser beam(488nm wavelength) with a 2mm spot size and with 10mW power was focused onto an entire ACF(1mm long, 10μ diameter) through focusing optics and a quartz window(see Fig.1). As shown in the figure, the beam covered the entire fiber, including a 1mm interval between the two electrodes. The laser power was varied in the range 1-40 mW at each temperature 25,100,200 and 290K to determine the recombination kinetics. The number of incident photons on a fiber, for example in the case

of 10mW incident laser power, was on the order of $10^{14}$/sec.

## III. Results and Analysis

### A. Intrinsic conductivity

In this work, we use the term intrinsic conductivity to refer to the conductivity in the absence of light(dark current) and the term intrinsic carriers is used to denote the carriers present in the absence of the light excitation. In the measurements of the temperature dependence of the intrinsic conductivity $\sigma(T)$, a semiconductor-like positive temperature dependence for $\sigma(T)$ is found(see Fig.4). This kind of temperature dependence is also observed in other disordered carbons [2,4,6,12,14,19,20,47,48]. Table 2 shows room temperature conductivities of the ACFs and other disordered carbon materials. The magnitude of this conductivity and its temperature-dependence are similar to those of Saran carbon[1], active carbon rods [3], glassy carbons heat treated at about 1000-1100K[12] and anthracene chars[47]. The magnitude of the conductivity is higher than that of evaporated carbon films[5] but lower than that of vapor-grown carbon fibers[49] and PAN-based fibers[50].

One of the features of interest in Fig.4 is the nearly linear temperature dependence of the conductivity for all ACFs in the studied temperature range. On the other hand, the slight departure from linearity gives information on the conduction mechanism discussed in section IV. The dominant conduction mechanism in this material seems to be a thermal activation process in the studied temperature range. However at low temperatures(below $\simeq$40K), the conduction due to the thermal activation will be small and then hopping of carriers from one localized state to another(variable range hopping) will be dominant[51]. In this case, more disorder facilitates the hopping of carriers as the defect state density near the Fermi level increases and the defects involved in the hopping process come closer to one another. Looking at the low temperature regime in Fig.4, the fibers with more disorder(i.e., more specific surface area) have the higher conductivities. On the other hand, at high

temperatures the thermal activation process will be dominant, as the carriers acquire sufficient energy to overcome the activation barrier. According to these arguments, the activation energy related to disorder will decrease, in agreement with the experimental observations. Thus, for the fibers with more disorder, the probability of overcoming the activation barrier increases at high temperatures. According to this conduction mechanism, the conductivity is expected to be zero at 0K. However in Fig.4, this trend for the behavior of $\sigma(T)$ at lower temperatures is not clearly identified so that a lower temperature measurement is required to confirm the expected conductivity behavior in the low temperature limit. A fit to the $\sigma(T)$ data using these models is discussed further in section IV.

B. Photoconductivity

In contrast with the intrinsic electrical conductivity, the photoconductivity exhibits a negative temperature dependence for all the ACFs that were investigated (see Fig.5). This result is consistent with the lower concentration of intrinsic carriers at low temperatures, thus lowering the recombination probability, and increasing the photoconductivity. Also of interest in Fig.5 is the observation that the fibers with higher surface area also have higher photoconductivities. This fact suggests that the same basic conduction mechanism is operative for the photoconductivity as for the intrinsic conductivity. Namely, the photocarriers are also in localized states and the fibers with more disorder have a smaller hopping range which leads to the higher conduction. Thus the temperature dependent photoconductivity curves in Fig.5 are consistent with the temperature dependent $\sigma(T)$ curves in Fig.4.

The transient curves for various light intensities all show an exponential rise and fall, as in Fig.6 where results are shown for the FR15 fiber. Similar values for the rise and decay time of the photoconductance are observed for other fibers. The simple exponential rise and decay curves with no additional structure imply that the energy of the trap states engaged in the decay process is limited to a narrow energy range around the Fermi level. If there

were both shallow and deep trap states involved in the photoconduction process, then the rise and decay curves would consist of two or more parts with different time constants.

The long decay times of about 0.3sec in Fig.7 indicate that a high density of trap states is involved in the recombination process because the lifetime of free carriers is generally much shorter, e.g., on the order of $10^{-3}$-$10^{-8}$ seconds[52]. The long decay times are further not significantly influenced by the magnitude of the specific surface area. The observed decay time is usually much longer than the lifetime of free photocarriers because the residence time in trap states is long. In disordered materials, a high density of trapped states is expected, making the excited photocarriers rather immobile. In fact, a decay time of several seconds was previously observed for a deposited carbon film[6]. A similar magnitude of decay time(0.05-0.1sec) was reported for a graphite fiber[53]. Another feature in Fig.7 is that the decay times are only weakly temperature dependent, with a slight increase in decay time observed with decreasing temperature except for the FR10 fiber, for which the decay time is $\simeq$0.3sec.

The kinetics of the recombination process in the ACFs is different from that given in a previous report on an evaporated carbon film[6] and a graphite fiber[53] where only the bimolecular recombination process was observed. The bimolecular recombination process is observed generally when the intrinsic carrier density is small and the photocarrier density becomes dominant(e.g., in insulators)[42]. Figure 8 for the FR15 fiber shows the dependence of photoconductivity on the laser intensity on a log-log scale for various temperatures (the other fibers exhibit the same trend). The significance of this figure is that it shows a change in the recombination kinetics according to the power law dependence for the photoconductivity, $\Delta\sigma \propto P^{\alpha}$ where $\Delta\sigma$ is the photoconductivity and P is the incident laser power. If $\alpha$=1, the recombination process is monomolecular, while an exponent $\alpha$=0.5 indicates a bimolecular process. In general, a monomolecular process implies that the density of the intrinsic carriers is much higher than that of photocarriers[42] so that the recombination is limited by the photocarrier density. The inserted triangles

in Fig.8 indicate the slopes corresponding to the monomolecular and bimolecular processes. In the bimolecular process, recombination is limited by the availability of photogenerated holes to recombine with the photoelectrons, so that recombination is proportional to the product $\Delta n \Delta p$ where $\Delta n = \Delta p$. In contrast to the previous result for disordered carbon films[6], Fig.8 clearly shows a monomolecular process( $\alpha = 1.0$) at high temperatures, while the onset of a bimolecular process ( $\alpha = 0.5$) can be seen at low temperatures and at high laser powers. At 290K, the monomolecular process( $\alpha = 1.0$) is dominant at all laser powers shown. As the temperature is decreased, the slope decreases indicating that the bimolecular process ( $\alpha = 0.5$) becomes increasingly important and the monomolecular process ( $\alpha = 1.0$ ) becomes less important. A typical case demonstrating the bimolecular process is the regime at 25K with the laser power above 4mW, where the slope is close to 0.5 and the bimolecular process appears to be dominant. Slopes between 0.5 and 1.0 are observed for most of the data at ≈100K, suggesting that the contribution of the monomolecular process is comparable to that of the bimolecular process. This trend that the bimolecular process becomes dominant at low temperatures and at high laser powers is reasonable because the density of photocarriers becomes dominant relative to the intrinsic carrier density under those conditions.

Figure 9 shows more clearly the change in recombination kinetics. In this figure, the power (in $\Delta\sigma = AP^{\alpha}$ ) is plotted versus the laser power P at each temperature, where A is a constant. In our experiments, the monomolecular process( $\alpha = 1.0$) was observed at high temperatures. This is consistent with the fact that the intrinsic conductivity is much larger than the photoconductivity at high temperatures. On the other hand, at low temperatures where the photoconductivity is comparable to the intrinsic conductivity, the power approaches $\simeq 0.5$. This phenomenon suggests that the dominant carriers in the material are photocarriers at low temperatures, and as a result the main recombination process occurs between the photocarriers (i.e., between the photoelectrons and photoholes ). In our experiments, both types of recombination kinetics were observed (see Fig.9) since the relative dominance

of the intrinsic carrier concentration and of the photocarriers could be reversed, depending on the choice of incident laser power and on the temperature.

The magnitudes of the dependence on laser power of the photoconductivity $\sigma(T)$ relative to room temperature are shown in Fig.10(for the FR15 fiber) for three different temperatures. This figure indicates that the dependence on laser power becomes smaller with increasing temperature. If the data are extrapolated to high laser power levels, the temperature-dependence would disappear at around 100mW. At 100mW where the photoconductivity is essentially temperature-independent, the density of intrinsic carriers is negligible compared to the photocarriers induced at that power level ($\simeq 10^{15}$ photons/sec per fiber). In contrast, at low laser powers where the density of the induced photocarriers is small, the photoconductivity is rather temperature-dependent.

We note that the observed increase in conductivity during the laser pulse is not caused by a heating effect. If a heating effect caused the increase in conductivity, changes in the recombination kinetics would not be observed. Furthermore, a temperature rise caused by a heating effect would produce an almost temperature-independent increase in the conductivity. Because the $d\sigma/dT$ is nearly constant as seen in Fig.4, a constant conductivity deviation would be observed, provided that the temperature rise by the laser incident is near constant over the studied temperatures. However in fact, the experiments show that the conductivities (Fig.5) change by a factor of several over the temperature range 30-290K. For these reasons, we believe that the effect is not a heating effect but rather a photoeffect. However, it may be difficult to distinguish a heating effect from a photoeffect if the heat exchange process occurs on the same time scale as the photocarrier recombination process.

## IV. Discussion

We have fit the temperature-dependent conductivity data to investigate the intrinsic conduction mechanisms. Figure 11 shows the fit of a model where two

terms are assumed, a constant term and a temperature dependent term, i.e., $\sigma = \sigma_{hop} + \sigma_{act}$. The first term $\sigma_{hop}$ is associated with the variable range hopping process, but appears to be temperature independent above ≈30K for the ACFs studied in the present work. The temperature dependent term $\sigma_{act}(=\sigma^{\circ}_{act} \exp(-E/kT))$ is written as a simple activation term. The fits for the various fibers to this functional form are shown in Fig.11 and values for $\sigma_{hop}$ and $\sigma_{act}$ are given in Table 3. The term due to the hopping conduction ($\sigma_{hop}$) is found to increase strongly with increasing specific surface area(SSA), though we have not been able to find the functional dependence of $\sigma_{hop}$ on SSA. The temperature-dependence of the intrinsic conductivity then comes from the temperature-dependent term($\sigma_{act}$) based on a thermal activation process. From the fits in Fig.11 we see that the activation energy E decreases with increasing SSA, but because of the exponential dependence on E, the effect of increasing the SSA is quite large. The net effect is that the temperature dependent term increases more rapidly with SSA than $\sigma_{hop}$. For example, the magnitude of $\sigma_{hop}$ at room temperature is only 15-25% of $\sigma_{act}$ for all the fibers. At high temperatures, satisfactory agreement between the data and the model is shown in Fig.11, although the fit is not good at low temperatures. In terms of the prefactor $\sigma^{\circ}_{act}$ of the thermal activation term $\sigma_{act}$, an increase (from 23.0 to 45.6S/cm) with SSA (from 1000 to 2000$m^2/g$) is observed. Since the prefactor becomes large as the inelastic collision length decreases[51], this trend for the prefactors is reasonable. From the magnitudes of the prefactors, an approximate inelastic collision length is estimated to be 15-30Å, following the equation[51] that the prefactor is about $0.03e^2/\hbar L_i$ where $L_i$ is a inelastic collision length. However, we could not distinguish whether this activation process is based on a nearest hopping of carriers or on a simple activation of trapped carriers to excited states because these two functions have the same form of exp(-E/kT).

With regard to the mechanism for the increase in the photoconductivity at low temperatures(Fig.5), an increase in the photocarrier concentration based on a increase in the lifetime is required. There are two explanations for the

increase in the lifetime. One explanation is that a decrease in the mobility of the photocarriers at low temperatures leads to a lower recombination rate, resulting the longer lifetime. If carriers are less mobile, the probability for carriers to meet each other and to recombine is reduced. In this model all the carriers of the appropriate sign are assumed to be equally involved in the recombination process. The other explanation is that thermally excited intrinsic carriers play a main role in the recombination process. In this model specific mobile carriers control the recombination process. Because the concentration of these excited carriers is temperature dependent, the decrease in the concentration of these carriers at low temperatures leads to a lower recombination rate, resulting in a longer lifetime of the photocarriers. It is difficult to specify here which mechanism is dominant. It depends on whether the states of the carriers in this disordered carbon are all localized or whether they have some extended states.

At low temperatures, the density of photocarriers is expected to become very large because of their long lifetime. The photoconductivity, however, is expected to show a decrease as the temperature is lowered further because the carriers become more immobile, and because the density of photocarriers eventually reaches a finite value depending on the laser power. In fact, the FR10 fiber shows a saturation effect below 50K in Fig.5. This idea predicts that the photoconductivity and the intrinsic conductivity will eventually become zero at 0K.

Assuming an appropriate value of the mobility, it is possible to estimate the densities of the intrinsic carriers and of the photocarriers. For the mobility in the localized states, $1cm^2/Vsec$ is assumed based on the calculated mobility of a phenol resin [54] for which the conductivity and the heat treatment temperature were about the same as for the ACFs in this work. Then the density of the intrinsic carriers and of the photocarriers at room temperature are estimated to be $\simeq 10^{21}/cm^3$ and $\simeq 10^{20}/cm^3$ (in case of 10mW laser power), respectively, assuming the majority of carriers exist in trapped states. This magnitude of the intrinsic carrier density is comparable to the

value of around $10^{20}/cm^3$ obtained by the Hall measurements and ESR[54] of a phenol resin. These values are also reasonable because Fig.10 indicates that about 100mW of incident light would generate a higher photocarrier density than the intrinsic carriers.

## V. Conclusions

Measurements of the intrinsic conductivity and the photoconductivity of activated carbon fibers have been carried out over the temperature range 30-290K. The temperature dependence is positive for the intrinsic conductivity and negative for the photoconductivity. The decay time of the photoconductivity is about 0.3sec. The recombination kinetics change from a monomolecular process to a bimolecular process with decreasing temperature and increasing photon intensity. It is assumed that most intrinsic carriers and photocarriers exist in a high density of localized states in this material. The main conduction mechanism is assumed to be variable range hopping at low temperatures and at high temperatures either short range hopping or thermal activation of carriers. An activation energy of about 20meV for the temperature-dependent term in the intrinsic conductivity fits the experimental data well at high temperatures. The density of the intrinsic carriers and the photocarriers at room temperature are estimated to be $\simeq 10^{21}/cm^3$ and $\simeq 10^{20}/cm^3$ (in the case of 10mW laser power), respectively. Both the intrinsic conductivity and the photoconductivity are expected to approach zero as $T \rightarrow 0K$. We have found that photoconductivity measurements, in combination with conductivity measurements, provide valuable information for understanding of the electronic properties of disordered carbon materials.

Acknowledgments

We would like to thank Dr.G.Dresselhaus, Professor M.Endo for enlightening conversations, Dr.A.Rao for help with the experiments, and A.Fung and S.diVittorio for both. We gratefully acknowledge support from Sumitomo Metal Industries(K.K) and Lawrence Livermore Laboratory Subcontract #B130530(M.S.D).

†Permanent Address: Advanced Carbon Research Laboratory, Sumitomo Metal Industries Ltd., Sunayama 16, Hasaki, Kashima, Ibaraki-ken, Japan

References

1. J.R.Dacey, D.F.Quinn and J.T.Gallagher, Carbon 4, (1966)73
2. R.McIntosh, R.S.Haines and G.C.Benson, J. Chem. Phys. 15, (1947)17
3. W.W.Smeltzer and R.McIntosh, Cann. J. Chem. 31, (1953)1239
4. M.D.Blue and G.G.Danielson, J.Appl.Phys. 28,(1957)583
5. T.Hanawa and J.Kakinoki, Carbon 1, (1964)403
6. J.M.MacFarlane, I.S.McLintock and J.C.Orr, Phys. Stat. Sol.(a)3,(1970)K239
7. S.Mizushima and Y.Hirabayashi, Carbon 6, (1968)123
8. I.S.Mclintock and J.C.Orr, Carbon 6, (1968)309
9. V.R.Deitz and E.F.MacFarlane, Proceedings of the Fifth Carbon Conference, Vol.2, p219, Pergamon Press, Oxford (1963)
10. I.S.Mclintock and J.C.Orr, Carbon 5, (1967)291
11. H.Hirabayashi and H.Toyoda, Proceedings of the Fourth Carbon Conference, p227, Pergamon Press, Oxford (1961)
12. F.Carmona, P.Delhaes, G.Keryer and J.P.Manceau, Solid State Communi.14, (1974)1183
13. R.R.Saxena and R.H.Bragg, J. Non-Cryst. Solid 28,(1978)45
14. D.F.Baker and R.H.Bragg, Phys. Rev. B 28,4,(1983)2219
15. J.W.Armstrong, C.Lackson and H.Marsh, Carbon 2,(1964)239
16. B.D.McMichael, E.A.Kmetko and S.Mrozowski, J. Optical Society of America 44,1, (1954)26
17. P.L.Walker, L.G.Austin and J.J.Tietjen, Carbon 2, (1965)1710
18. Y.Maruyama and H.Inokuchi, Chem. Soc. of Jap. Bull. 39, 7, (1966)1418
19. E.A.Davis and R.F.Shaw, J. Non-Cryst. Solid 2, (1970)406
20. W.Bücker, J. Non-Cryst. Solid 12, (1973)115
21. S.Mrozowski, Phys. Rev. 77, (1950)838
22. S.Mrozowski, Carbon 3, (1965)305
23. S.Mrozowski, Carbon 6, (1968)841

24. S.Mrozowski, Phys. Rev. 85, (1952)609
25. S.Mrozowski, Carbon 9, (1971)97
26. S.Mrozowski, Carbon 11, (1973)433
27. S.Mrozowski, J. Low Temp. Phys. 35, (1979)231
28. H.Nagata and T.Yoshida, Chemical Economics, (1977 April)44
29. S.Ikegami and K.Shimazaki, Fuel and Combustion 54, 2 (1987)
30. N.Ishizaki, Chemical Engineering (1984 July)24
31. K.Tai and N.Shishido, Polymer Processing 35, (1986)384
32. G.N.Arons and R.N.Macnair, Textile Res. J. 42,(1972)60
33. E.Tanaka, Fuel and Combustion 54, 4, (1987)241
34. A.Yoshida, I.Tanahashi, Y.Takeuchi and A.Nishino, IEEE CHMT-10,1,(1987)100
35. N.Kasaoka, Y.Sakata, E.Tanaka and R.Naito, J. Chem. Soc. Japan, (1987)990
36. G.M.Nieh and D.T.Grow, J. Colloid Interface Science 119, 1, (1987)280
37. J.W.Herrick, in "23rd Ann. Tech. Conf.SPI Reinforced Plastics/Composites, 16A(1968)
38. Y.Komatsubara, S.Ida, H.Fujitsu and I.Mochida, Fuel 63,(1984)1738
39. I.Mochida, M.Ogaki, H.Fujitsu, Y.Komatsubara and S.Ida, Fuel 64,(1985)1054
40. G.G.Jayson, T.A.Lawless and D.J.Fairhurst, J. Colloid and Interface Science 86, (1982)379
41. K.Kaneko and N.Shindo, Carbon 27, 6, (1989)815
42. R.H.Bube,Photoconductivity of Solids, Wiley, New York, London, 1960
43. A.Rose, Concepts in Photoconductivity and Allied Problems, Interscience Publishers, New York, 1963
44. Photoconductivity and Related Phenomena, J.Mort and D.M.Pai edit, Elsevier, 1976
45. S.Mrozowski and A.Chaberski, Phys. Rev. 104, (1956)74
46. C.A.Klein, J. Applied Physics 35, 10, (1964)2947
47. P.Delhaes and F.Carmona, Physical Properties of non-crystalline carbons, Chem. Phys. Carbon 17 (1981)
48. S.diVittorio et al., unpublished
49. J.Heremans, Carbon 23,4,(1985)431

50. I.L.Spain, K.J.Volin, H.A.Goldberg and I.Kalnin, J. Phys. Chem. Solids 44, 8, (1983)839
51. N.Mott, "Conduction in Non-Crystalline Materials", Oxford University Press(1987)
52. N.W.Ashcroft and N.D.Mermin, "Solid State Physics", Holt, Rinehart & Winston(1976)
53. J.Steinbeck, G.Braunstein, M.S.Dresselhaus, G.Dresselhaus and T.Venkatesan, Extended Abstracts of Symposium K "Graphite Intercalation Compounds", 1986 Fall Meeting of the MRS, p129
54. W.Bücker, J. Non-Cryst. Solid 18, (1975)11

Figure Captions

Fig.1 Geometry of the ACF sample mounted on a mica substrate. The laser beam 10mW $Ar^+$ ion laser irradiates the indicated circular region(see inset) and $\simeq 10^{14}$ photons/sec are incident on the fiber.

Fig.2 Scanning Electron Microscopy photographs of a phenol-derived ACF. (a)cross section of a fiber, having a rather round shape and a smooth surface. (b)cross section with a higher magnification. The width of the crack-like openings is $\simeq 500$Å. The length scales in both photographs are given.

Fig.3 X-ray diffraction pattern of ACF(FR12).

Fig.4 Temperature dependence of the "intrinsic" electrical conductivity for the four types of fibers.

Fig.5 Temperature dependence of the photoconductivity for each of the fiber types.

Fig.6 Decay time of the induced photoconductivity for each of the four types of fibers as a function of temperature.

Fig.7 Decay curves of photoconductivity at the incident laser powers of 10, 4 and 1mW at 30K.

Fig.8 Photoconductivity dependence on irradiation power at various temperatures for the FR15 fiber, plotted on a log-log scale.

Fig.9 Change in recombination kinetics at various incident power level. $\alpha = 1$ and 0.5 implies a monomolecular process or a bimolecular process, respectively.

Fig.10 Change in the temperature dependence of the photoconductivity as a function of power level. An extrapolation to the high power limit indicates that the temperature dependence disappears(the ratio becomes unity for all temperatures shown) at 100mW.

Fig.11 Calculation of the "intrinsic" conductivities based on a conduction model. The insert indicates the conduction model schematically. The model consists of two terms based on a thermal activation process($\sigma_{act}$) and a hopping process( $\sigma_{hop}$). The hopping process is almost constant over the studied temperature range.

Table 1. Properties of phenol-derived activated carbon fibers

Table 2. Conductivity values for various disordered carbons

Table 3. Fitting values for the conductivity

Table 1. Properties of phenol-derived carbon fibers[33]

| | FR10 | FR12 | FR15 | FR20 |
|---|---|---|---|---|
| Specific surface area ($m^2/g$) | 1000 | 1200 | 1500 | 2000 |
| Pore radius (Å) | 9 | 10 | 12 | 16 |
| Pore volume ($cm^3/g$) | .22 | .35 | .50 | .75 |
| Benzene adsorption capacity (wt%) | 22 | 35 | 45 | 65 |
| Ash (wt%) | .03 | .03 | .03 | .04 |
| Conductivity at room temperature* (S/cm) | ≈10 | ≈20 | ≈25 | ≈35 |

* from this paper

Table 2. Conductivity values for various disordered carbons

| | $H_{TT}$(°C) | Conductivity(S/cm) | Reference |
|---|---|---|---|
| Saran carbon | ≈720 | 20–100 | 1 |
| Active carbon rods | ≈750 | ≈20 | 3 |
| Glassy carbon | ≈750 | 1–10 | 12 |
| | 800–1000 | 10–100 | |
| Evaporated carbon film | | ≈ 0.1 | 5 |
| Vapor grown carbon fiber | 1400 | ≈ 900 | 49 |
| | as grown | ≈ 500 | |
| Phenol-formaldehyde resin | 700–900 | 15–150 | 54 |
| Phenol ACFs | 800–1100 | 10–40 | this paper |

Table 3. Fitting values for the conductivity*

| | $\sigma_{hop}$(S/cm) | $\sigma_{act}$(S/cm) | |
|---|---|---|---|
| | | $\sigma^0_{act}$(S/cm) | E(meV) |
| FR10 | 2.2 | 23.0 | 24 |
| FR12 | 5.6 | 37.3 | 22 |
| FR15 | 7.9 | 39.6 | 21 |
| FR20 | 10.3 | 45.6 | 19 |

* fitting equation is

$$\sigma(T) = \sigma_{hop} + \sigma_{act} = \sigma_{hop} + \sigma^0_{act} \exp(-E/kT)$$

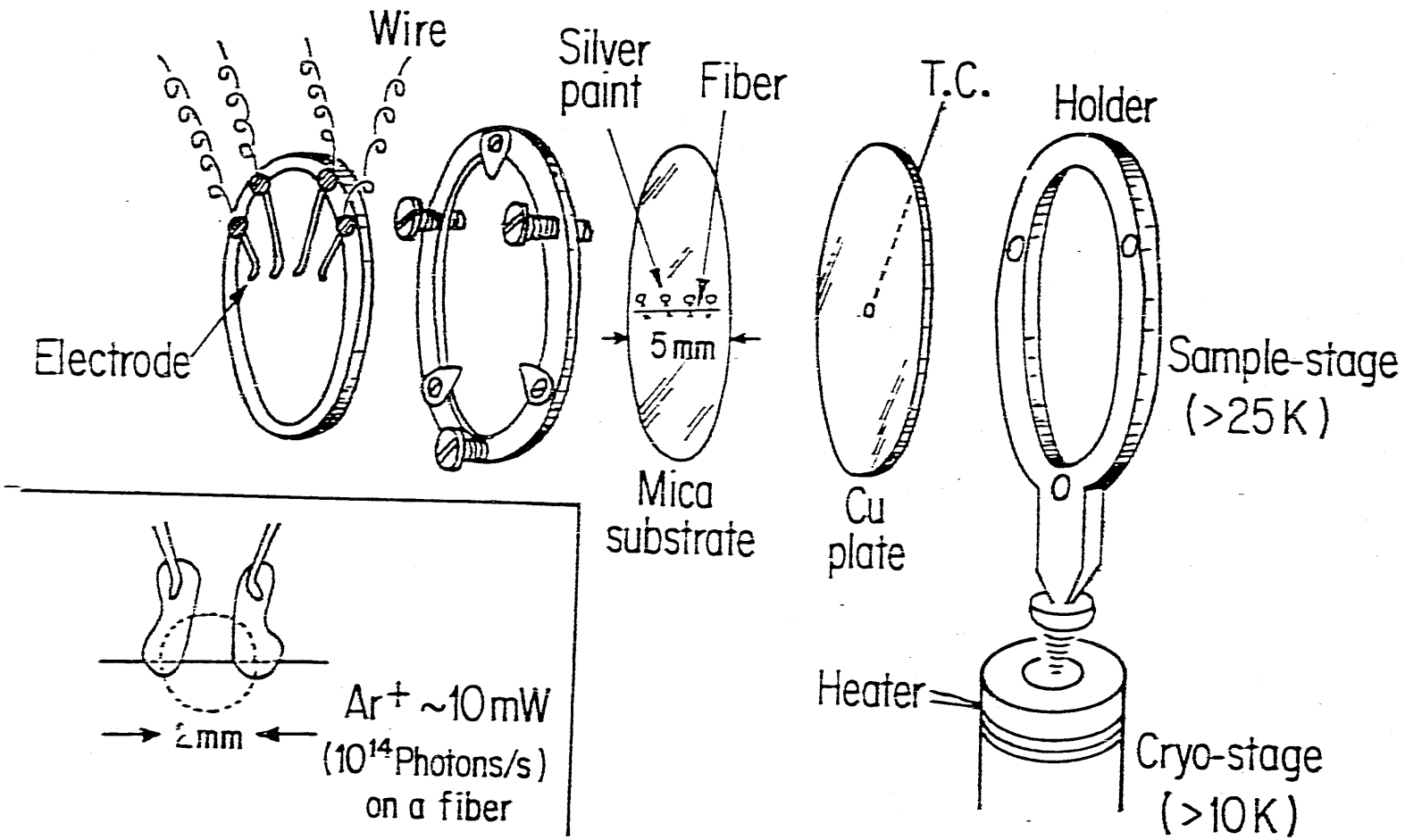


Fig.1 Geometry of the ACF sample mounted on a mica substrate. The laser beam ~10mW $Ar^+$ ion Laser irradiates the indicated circular region(see inset) and about $10^{14}$ photons/sec are incident on the fiber.

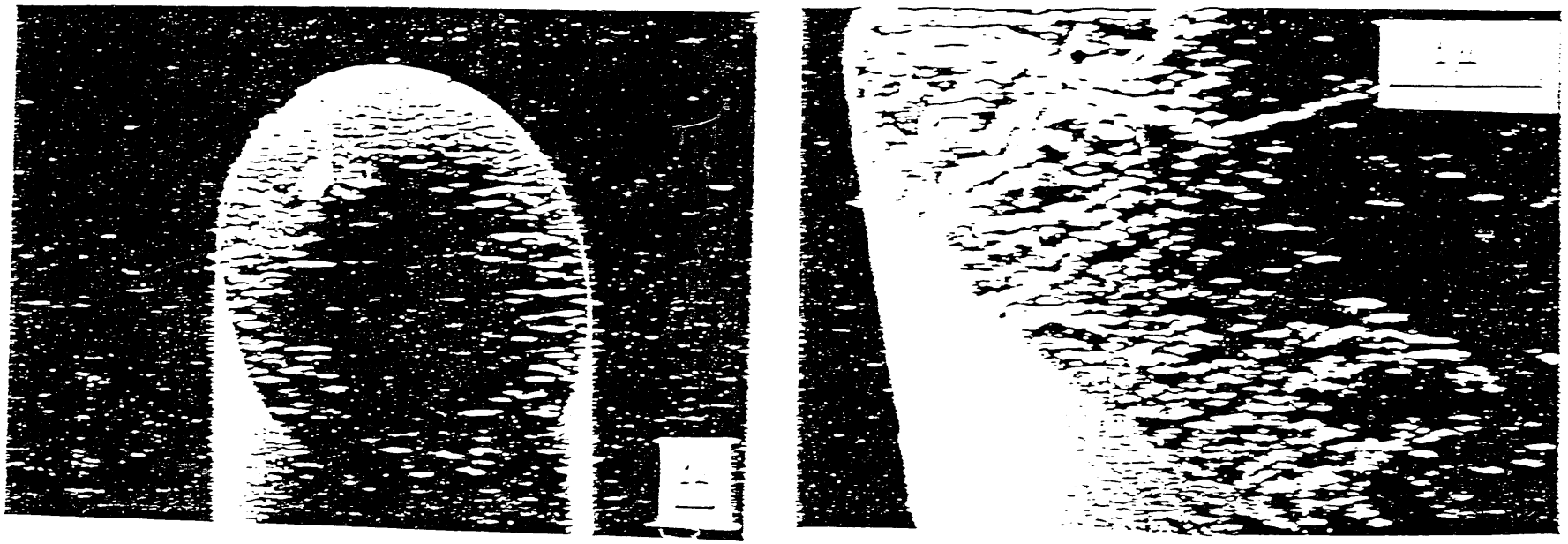

(a) (b)

Fig.2 Scanning Electron Microscopy photographs of a phenol-derived ACF. (a) cross section of a fiber, having a rather round shape and a smooth surface. (b) cross section with a higher magnification. The width of the crack-like openings is around 500Å. The length scales in both photographs are given.

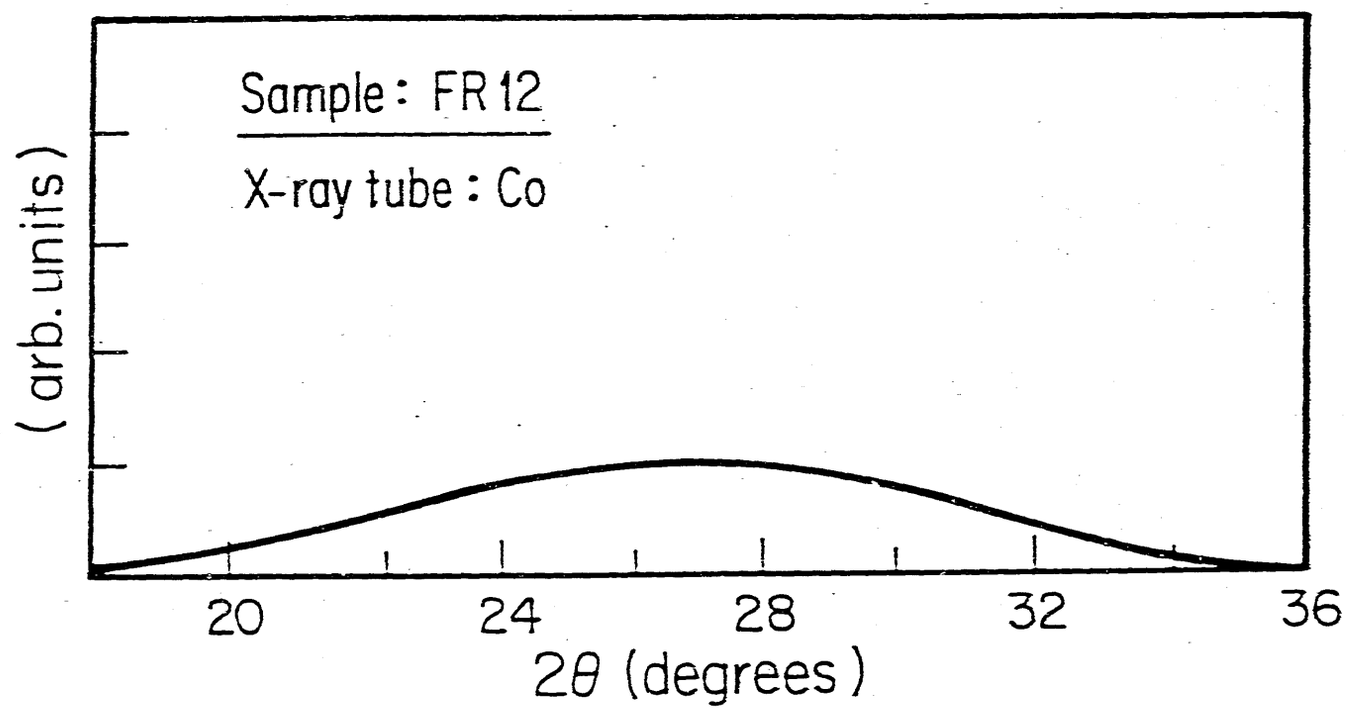


Fig.3 X-ray diffraction pattern of ACF(FR12).

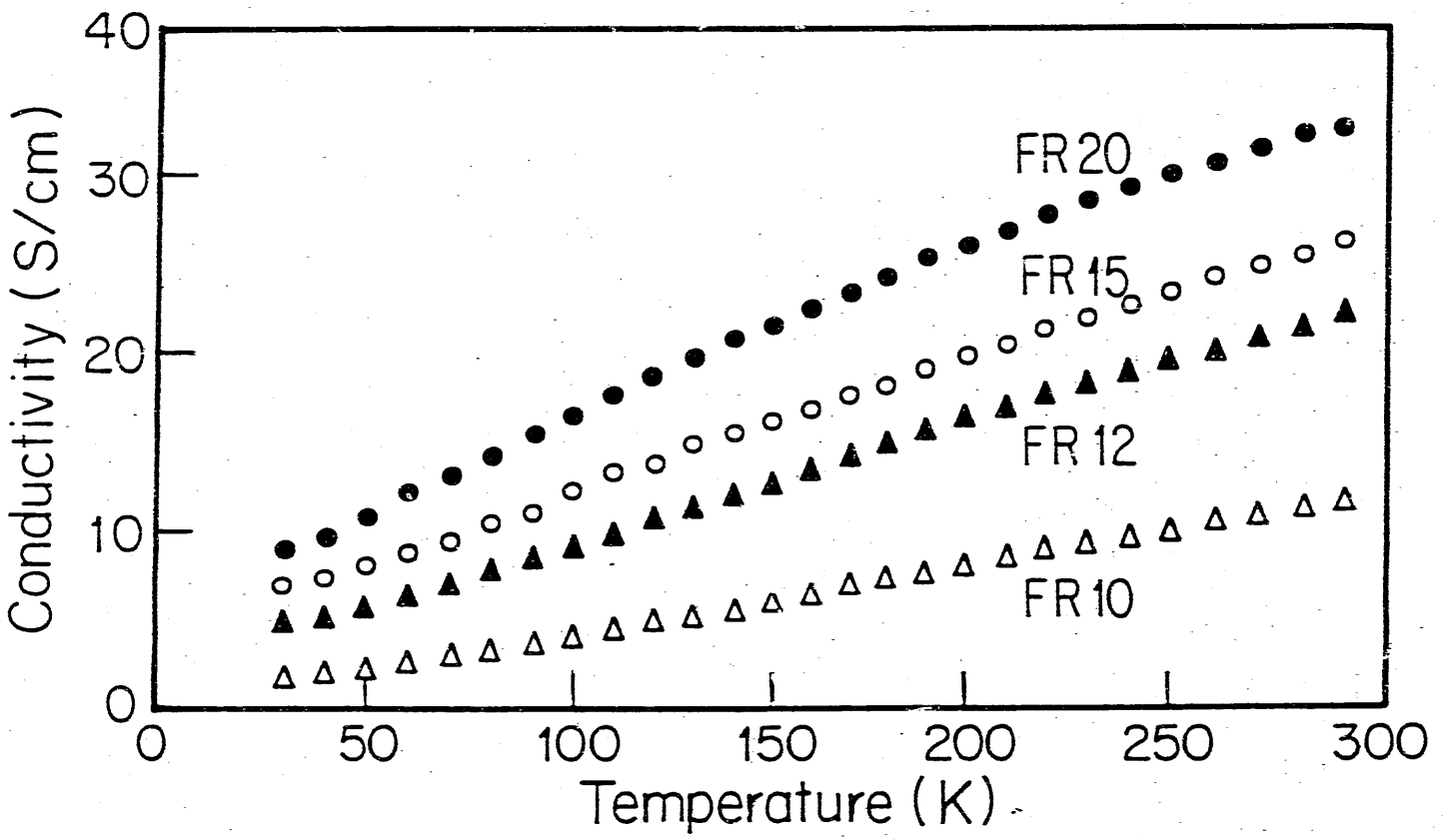


Fig.4 Temperature dependence of the "intrinsic" electrical conductivity for the four types of fibers.

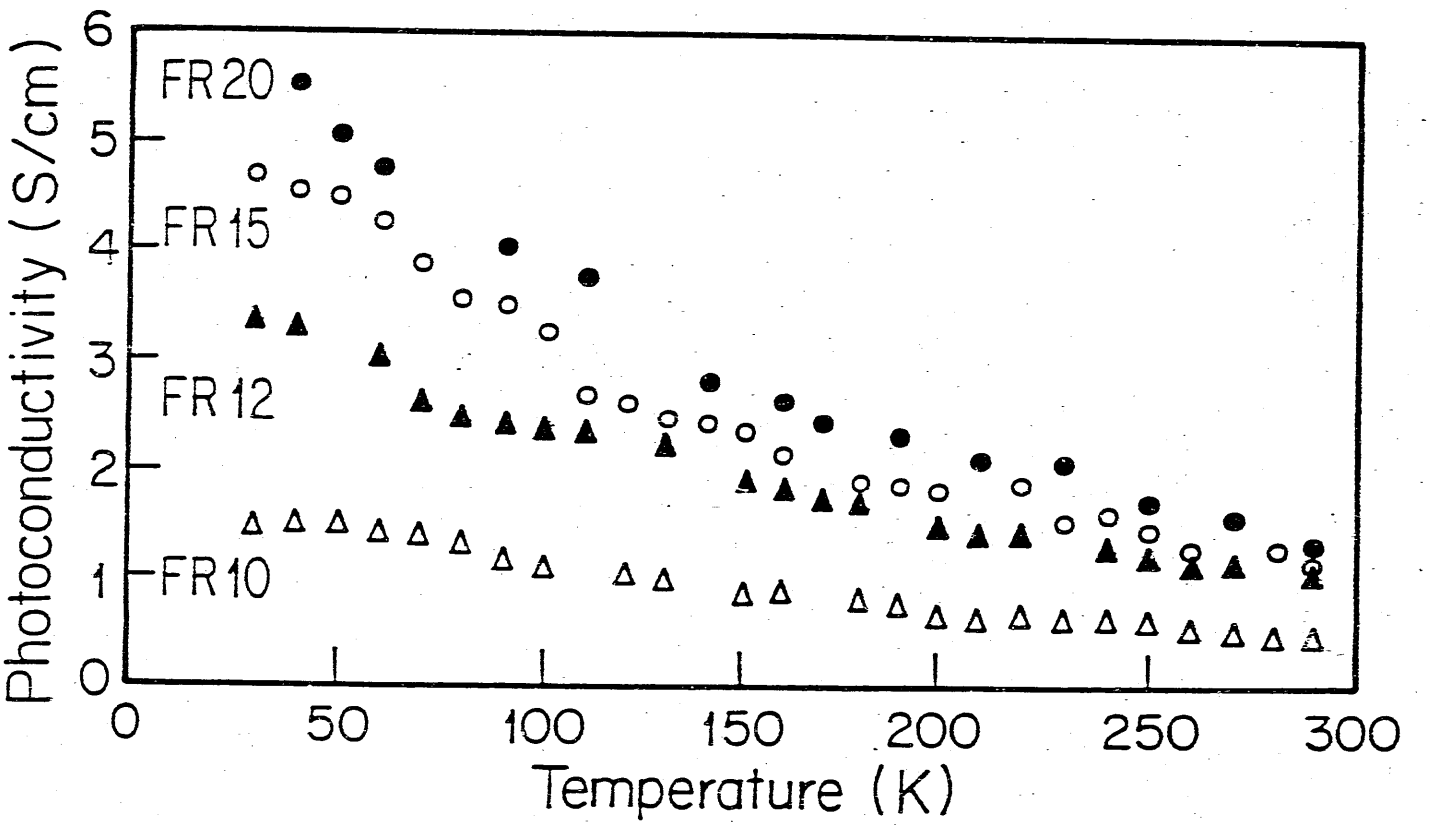


Fig.5 Temperature dependence of the photoconductivity for each of the fiber types.

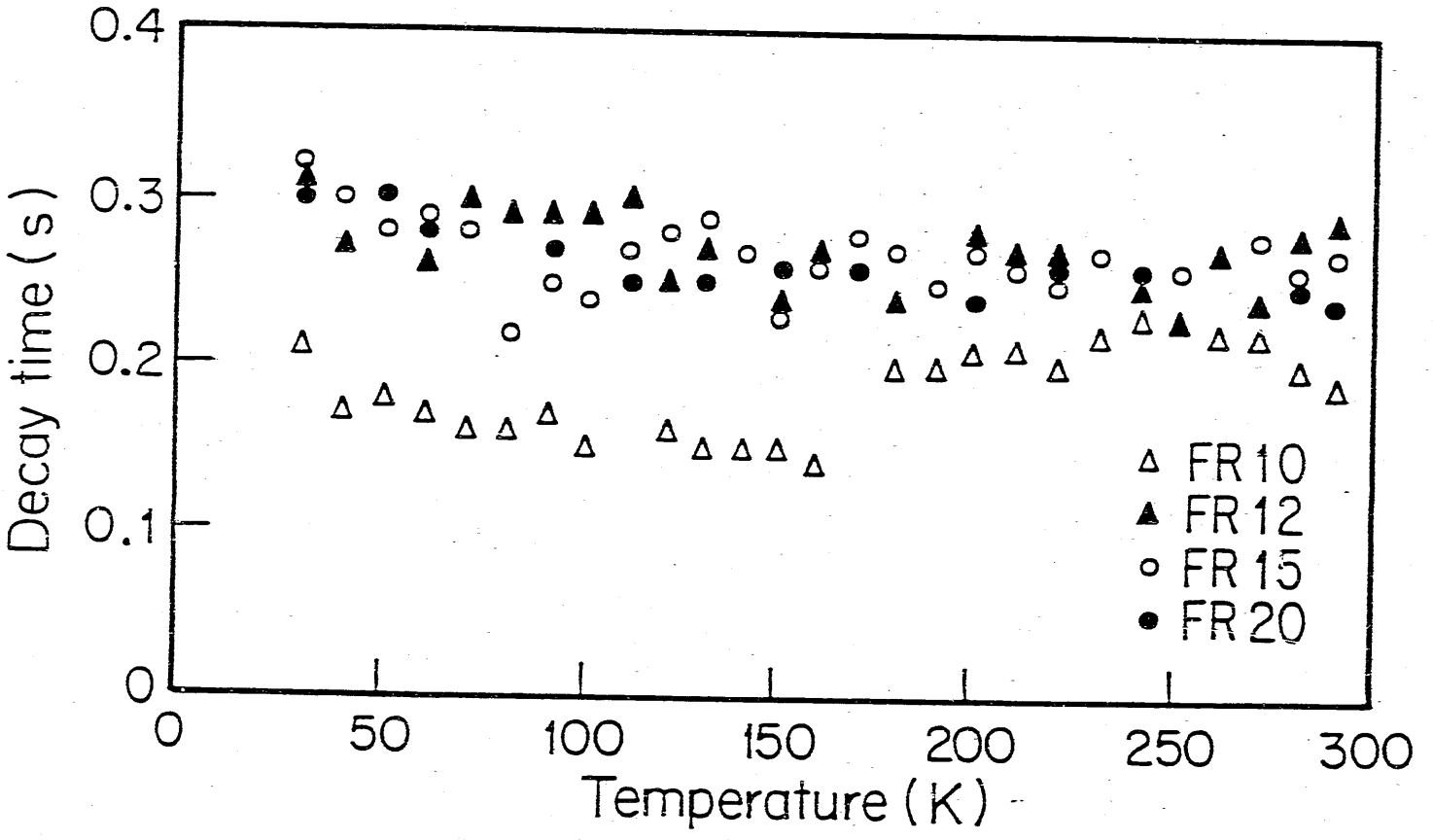


Fig.6 Decay time of the induced photoconductivity for each of the four types of fibers as a function of temperature.

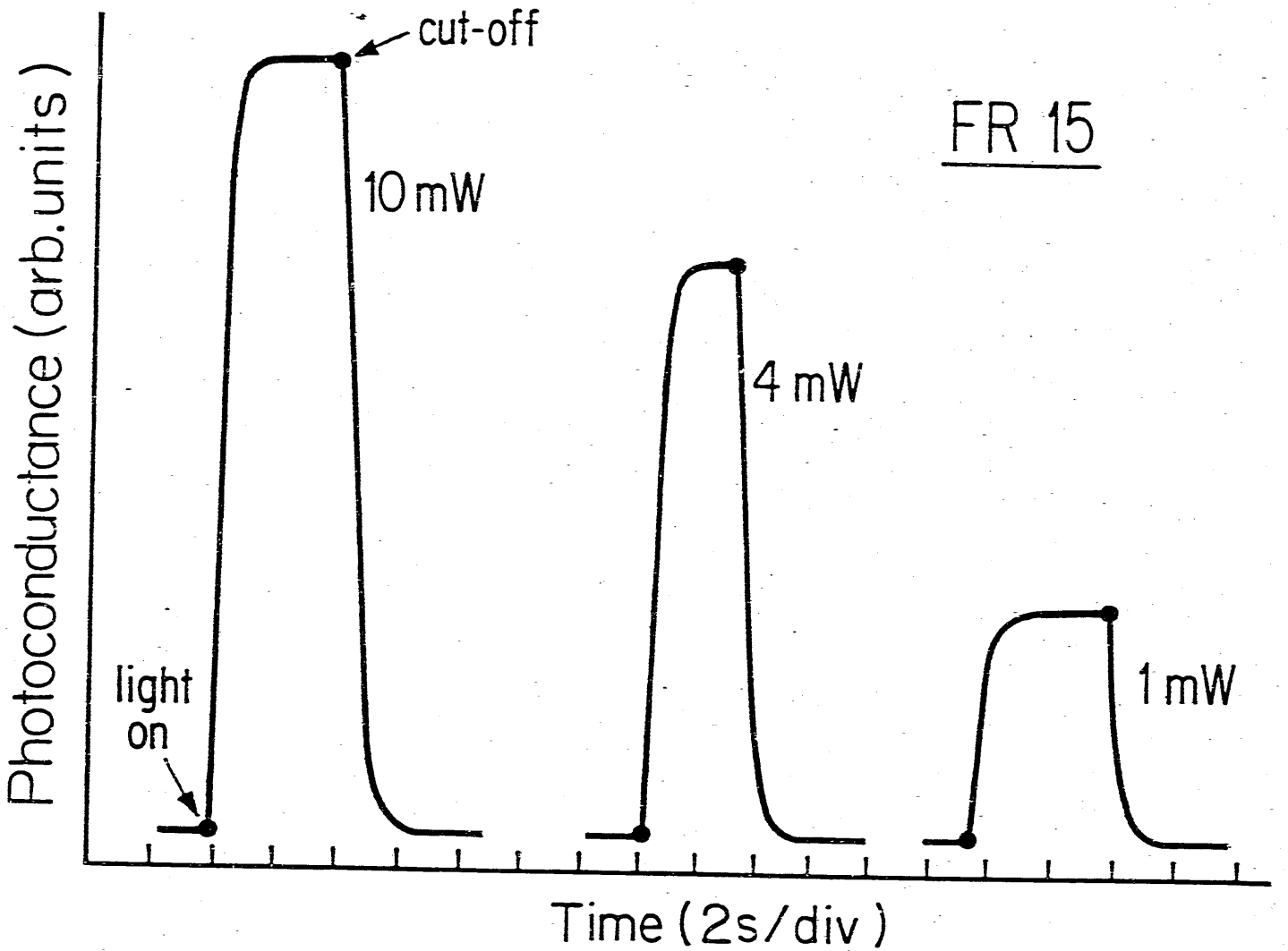


Fig.7 Decay curves of photoconductivity at the incident laser powers of 10, 4 and 1mW at 30K.

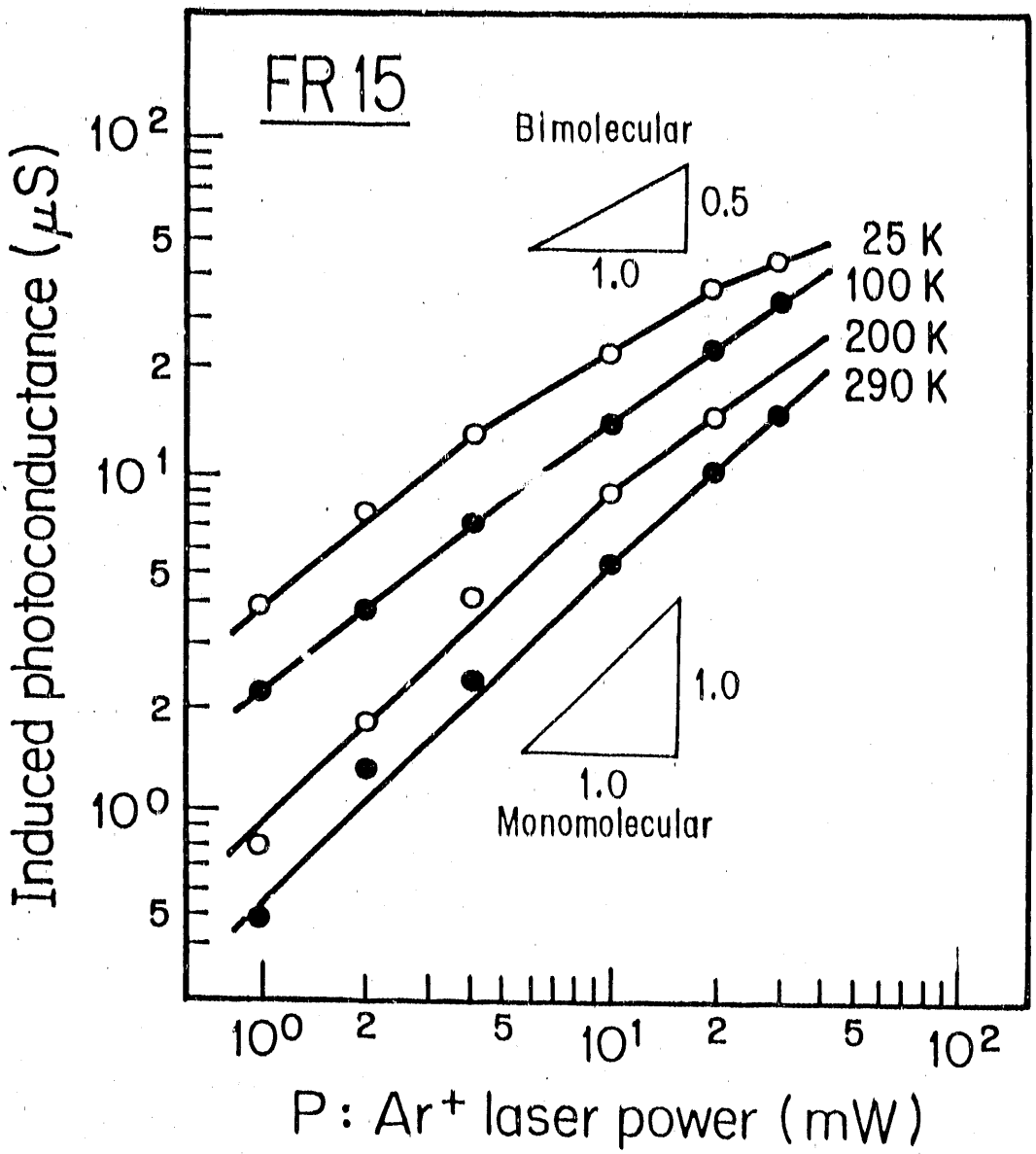


Fig.8 Photoconductivity dependence on irradiation power at various temperatures for the FR15 fiber, plotted on a log-log scale.

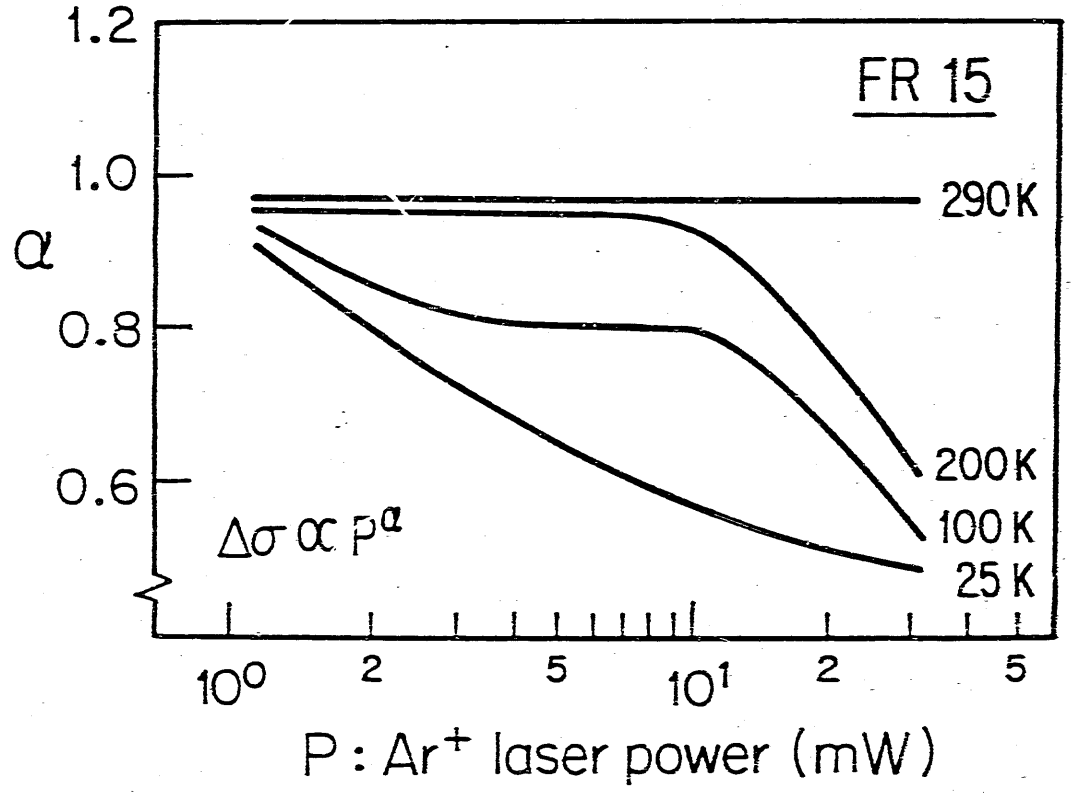


Fig.9 Change in recombination kinetics at various incident power level. $\alpha$=1 and 0.5 implies a monomolecular process or a bimolecular process, respectively.

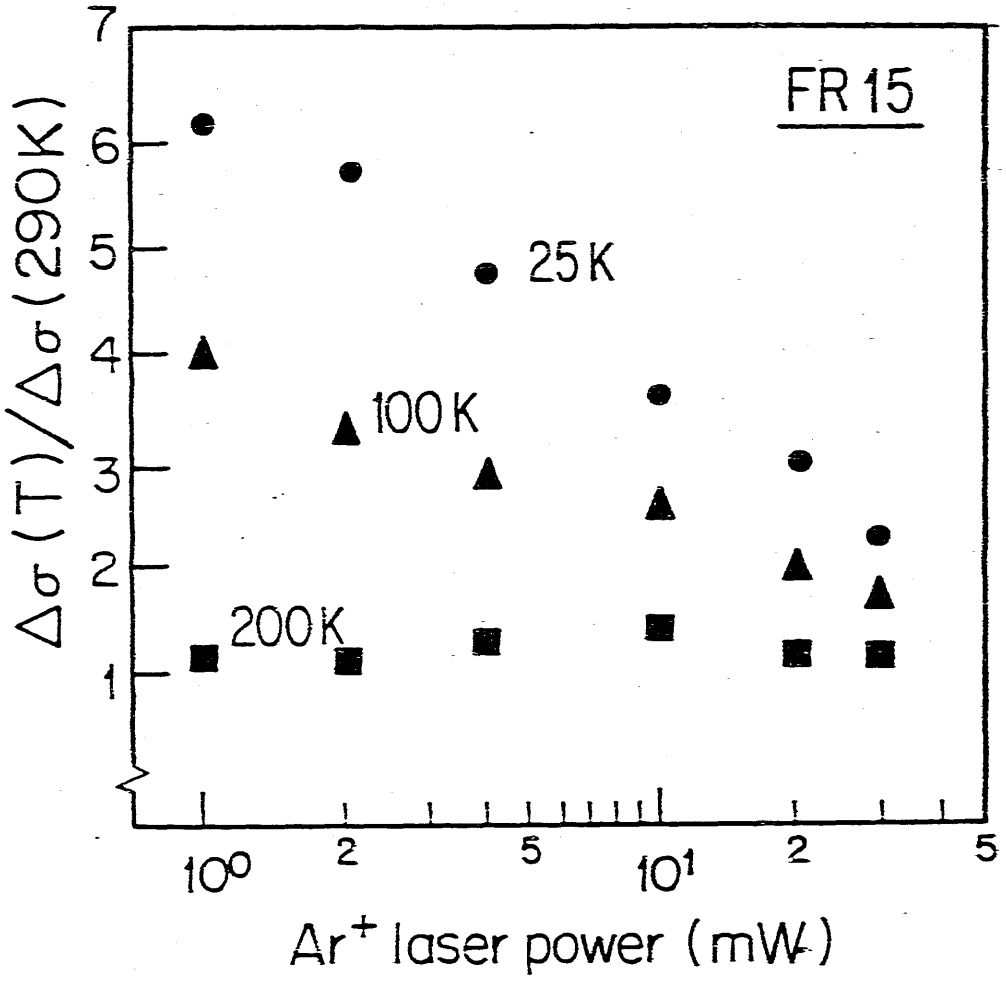


Fig.10 Change in the temperature dependence of the photoconductivity as a function of power level. An extrapolation to the high power limit indicates that the temperature dependence disappears(the ratio becomes unity for all temperatures shown) at around 100mW.

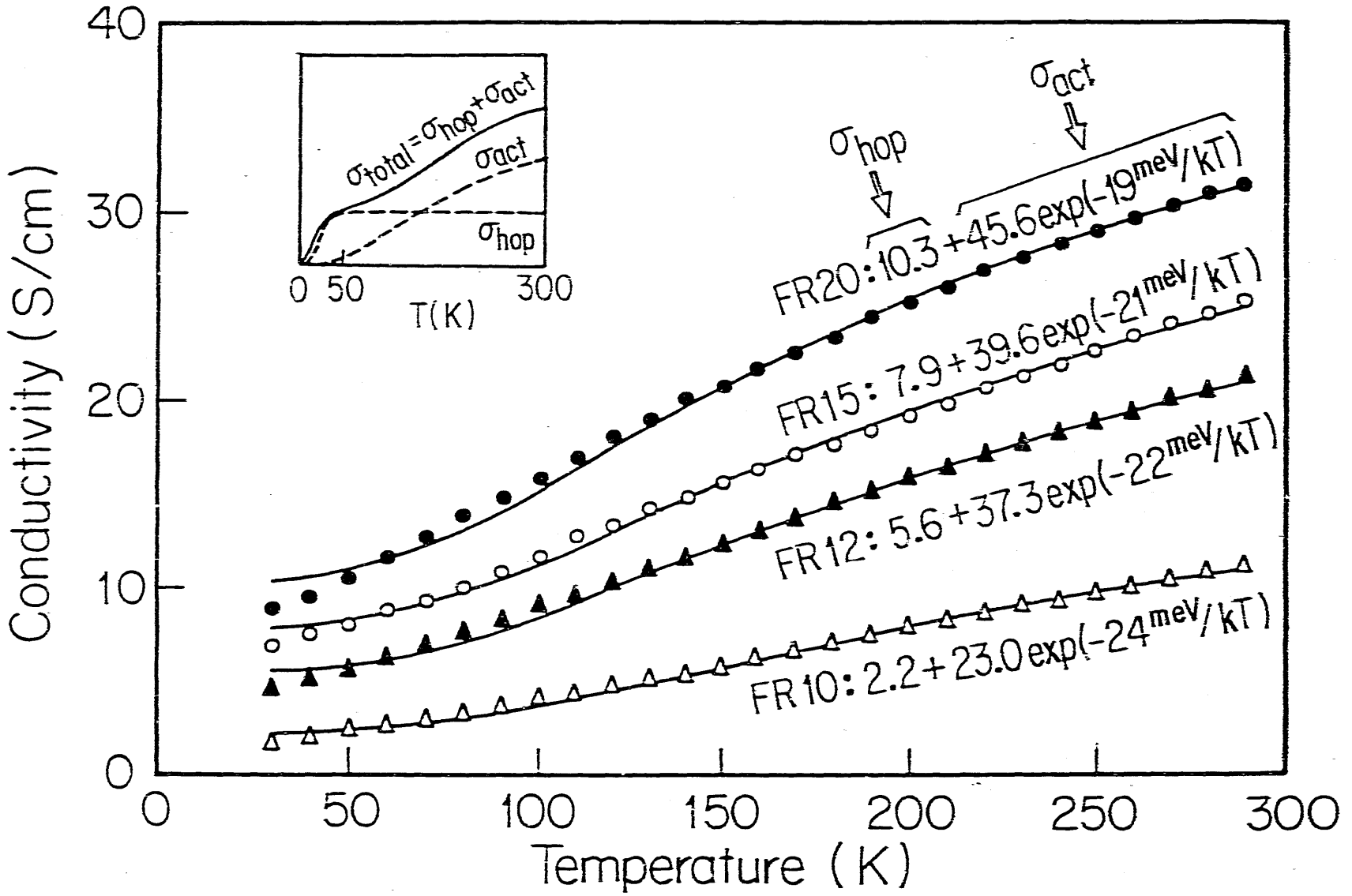


Fig.11 Calculation of the "intrinsic" conductivities based on a conduction model. The insert indicates the conduction model schematically. The model consists of two terms based on a thermal activation process( $\sigma_{act}$) and a hopping process( $\sigma_{hop}$). The hopping process is almost constant over the studied temperature range.

# -END-

# DATE FILMED

11/05/90